PHYSICAL REVIEW A VOLUME 24, NUMBER 2 AUGUST 1981

Dynamics of defects in Rayleigh-Bénard convection

Eric D. Siggia and Annette Zippelius
Laboratory of Atomic and Solid State Physics, Cornell University, Ithaca, New York 14853
(Received 19 March 1981)

The behavior of an extra roll extending into an otherwise regular convection pattern is studied as a function of Rayleigh number, Prandtl number, P, and wavelength, by means of a fully resolved numerical simulation of the Boussinesq equations with free-slip boundary conditions. For reduced Rayleigh numbers of order one or less and $P \gtrsim 40$, numerical simulations of the lowest-order amplitude equations reproduce the Boussinesq results semiquantitatively. In particular, we find that when this class of defects is stable, they move with constant velocity v, parallel to the roll axis and give rise to a slow modulation of the roll pattern of the form $f(x, y - vt)$. Both f and v have been calculated analytically within a linearized theory. The envelope function f depends in an essential way on v such that the limit $v \to 0$ cannot be sensibly taken.

I. INTRODUCTION

The onset of thermal convection in a layer of fluid heated from below is probably the best understood example of symmetry breaking and pattern formation in a nonequilibrium system.[1,2] The bifurcation is a forward or reversible one that permits one to treat the competition among various patterns analytically by a two-scale or Ginzburg-Landau-type perturbation theory in terms of a slowly varying amplitude function.[1,3-5] Near onset, within the Boussinesq approximation, it has been shown that the only stable convection patterns in an infinite system consist of a periodic array of two-dimensional roll pairs of opposite circulations. These patterns, for a given fluid, are uniquely characterized by a reduced Rayleigh number $\epsilon = (R - R_c)/R_c$, where R_c is the minimum value of R for which convection persists and a wave number q defined such that $2\pi/q$ is the spatial period. These conclusions are unchanged when the container is finite but periodically continued except that q is quantized.

Anyone who examines pictures of convection in large aspect ratio cells at moderate Rayleigh numbers, when the initial conditions are not controlled, would find a very disordered and in general nonstationary pattern.[6,7] There is an obvious analogy here to the defects one sees in certain liquid crystals or solids,[8] though in natural convection it is often difficult to tell where one defect ends and the next one begins. The simplest type of defect discernible in convection is an extra roll pair inserted into an otherwise ideal pattern. The position of this so-called dislocation is taken to be the point where the extra roll terminates. A number of authors have noted that dislocations can move into or out of a patch of ordered rolls and thereby provide a bulk mechanism for the adjustment of q.[6] Our intent here is to study the dynamics of dislocations in a sufficiently idealized setting where numerical and analytical calculations can be quantitatively compared.

There are several reasons for undertaking such an investigation beyond the very qualitative comparisons that might be made with the above experiments and the possibility of exploring how q is adjusted in bulk. Whitehead has done a controlled series of measurements in a large rectangular cell where he induced initially two domains of rolls with parallel axes and wavelengths in a ratio of 3:2.[9] The domain with the larger wavelength expanded at constant velocity at the expense of the other, while maintaining the interface between the two domains straight and perpendicular to the roll axis. The velocity in units of κ/d, where κ is the thermal diffusivity and d the layer depth, varied approximately linearly with $R - R_c$ and inversely with the Prandtl number $P = \nu/\kappa$, where ν is the kinematic viscosity.

A second reason for investigating defects is to better understand the dynamics of convection for small ϵ where a perturbative analytic theory is believed to apply. It is well known that the amplitude equations of Ref. 4 that describe the long-wavelength dynamics of an ordered roll pattern, do not allow for the generation of vertical vorticity, ω_z, and are unchanged if the nonlinear terms in the Navier-Stokes equations are omitted. It is also known that the convective terms in the Navier-Stokes equations vanish in the limit $P \to \infty$, κ finite, i.e., ω_z tends to zero with P^{-1}. Now a dislocation at finite P certainly generates vertical vorticity near its core; and in view of Whitehead's experiments, which showed its velocity to vanish with P^{-1}, one could reasonably infer that the presence of ω_z was necessary for any motion to occur. Higher-order terms in the amplitude expansion would then be required to account for the dislocation's velocity.

Both the production of ω_z and defects are

thought, although for slightly different reasons, to be relevant to the very low-frequency noise observed in large cells for $P \lesssim 1$ and at Rayleigh numbers where conventional stability analysis for an infinite system predicts no time-dependent motions.[10] The lateral boundaries almost certainly play some role in these phenomena, and one suspects that the patterns are nonideal, perhaps shifting, and contain defects.[11] Large scale changes in pattern seem to require vertical vorticity. Lastly, a component of ω_z appears at the bifurcation to oscillatory convection studied by Busse, and Clever and Busse.[12,13]

Contrary to our expectations, we found that the amplitude equation of Ref. 4 accounts at least semiquantitatively for the motion of an isolated dislocation near onset provided it is stable. There is no qualitative effect that can be attributed to ω_z and a finite P, although the variation in velocity with P for $P \lesssim 60$ is much greater than the amplitude expansion can account for. None of our results are in direct conflict with Whitehead's experiments. However, for parameters other than those that were directly measured, the dislocation motion is very different from what one would have inferred. Irrespective of any relationship to experiments, we believe it is still of interest to present a quantitative comparison between a full numerical simulation of both the Boussinesq and the amplitude equations, and analytic calculations for a nontrivial flow.

In Sec. II, we present our simulations of the amplitude and the Boussinesq equations under identical boundary conditions. Since both codes can be run with the same input parameters, geometrical effects can be factored out of the comparison. Section III contains our analytic solution of the linearized amplitude equations for an isolated dislocation in a large container and comparison with numerical results. In the conclusion, we return to the experiments, and comment on the possible effects of lateral boundaries.

II. NUMERICAL PROCEDURES AND RESULTS

Our numerical simulations have all been performed with free-slip boundary conditions top and bottom and periodic ones laterally. These assumptions both simplify the numerical algorithms as well as facilitate comparison with analytic theory. Since our goal is to understand the motion of an isolated dislocation near onset, periodic lateral boundary conditions are more effective than rigid ones in minimizing the influence of the "walls" on the bulk for a fixed investment of computer time. The form of the amplitude equation in Ref. 4 is independent of whether the top and bottom surfaces are rigid or free slip.[4,5] However, higher-order terms have only been calculated for the free-slip problem, which argues in favor of using the same boundary conditions in the numerical simulations.[14] It is relatively easy to impose rigid lateral boundary conditions on the amplitude equations, and with the understanding we have achieved about the behavior of defects in isolation, it would make good sense to include wall effects at the level of the amplitude equations. We will always work in units for which the depth of the fluid layer d and the thermal diffusivity κ equal one.

The Boussinesq equations were fully simulated with a pseudospectral code of conventional construction. For $2 \leq P < 20$ four vertical modes, $\sin(n\pi z)$ or $\cos(n\pi z)$, $n = 0, 1, 2, 3$, were judged adequate for $\epsilon \leq 0.5$ and marginal for $\epsilon = 1$. For larger P, one could go a factor of 2 higher in ϵ with the same vertical resolution. In the lateral directions, 6–8 Fourier modes per roll pair, i.e., 3 or 4 harmonics of the basic wave number, were adequate to completely describe the flow and eliminate aliasing. The defect velocity, temperature and velocity spectra, and the temperature and vorticity fields in real space, were all compared for the same flow under a variety of different resolutions to ensure against errors from this source. At a marginal resolution, with four modes in z and $P = 20$, $\epsilon = 2$, the mean-square temperature (velocity) variance that would otherwise fall in higher modes was 0.5% (0.1%) of the total while the defect velocity was in error by a few percent. The maximal allowed time step increased as ϵ decreased until $\epsilon \simeq 0.5$ whereupon it saturated.

At infinite P, the nonlinear and time derivative terms, which in dimensionless units are multiplied by P^{-1}, can be dropped from the Navier-Stokes equations so that the velocity becomes an instantaneous function of the temperature. In comparison with $P = 100$, our memory requirements are nearly halved and the computation time necessary to simulate one unit of physical time is decreased by a factor of order 10. Most of the last factor came from a larger time step. About 5 h of Cray time were spent on this project and the largest runs required 4×10^5 words of memory.

The amplitude equation, for complex A, was simulated in dimensionless scaled form,[4,5]

$$\frac{\partial A}{\partial t} = A + \left(\frac{\partial}{\partial x} - i\frac{\partial^2}{\partial y^2}\right)^2 A - |A|^2 A. \tag{2.1}$$

TABLE I. The scaling factors required to convert the length and time scales in Eq. (2.1) (denoted by an overbar) to physical units with $\kappa = d = 1$ (Refs. 4 and 5). We define $\bar{x} = x/\xi_{\parallel}$, $\bar{y} = y/\xi_{\perp}$, $\bar{t} = t/\tau$, $\epsilon = (R - R_c)/R_c$, and $\xi_{\perp}^2 = \xi_{\parallel}/(2q_0)$, where q_0 is the wave vector of the first unstable mode at $R = R_c$.

	q_0	$\xi_{\parallel}$	τ
free slip	$\pi/\sqrt{2}$	$[8/(3\pi^2\epsilon)]^{1/2}$	$(1+P)/(1.5\pi^2\epsilon P)$
rigid	3.117	$(0.148/\epsilon)^{1/2}$	$(0.5117+P)/(19.65\epsilon P)$

To return to physical variables for either rigid or free-slip boundary conditions, one has merely to restore the scaling factors listed in Table I. The reduced Rayleigh number ϵ only enters (2.1) implicitly through the initial conditions and a scaled box size. The physical fields such as the temperature may be recovered from relations of the form

$$T(x, y, t) = \lambda\epsilon^{1/2}\mathrm{Re}[A(x/\xi_{\parallel}, y/\xi_{\perp}, t/\tau)e^{iq_0x}] \times \sin(\pi z) + O(\epsilon),$$

where λ is a numerical factor dependent on the boundary conditions and x, y, z and t are in physical units, $\kappa = d = 1$. It will be very convenient in what follows to recast (2.1) in the form

$$\frac{\partial A}{\partial t} = -\frac{\delta F}{\delta A^*}, \tag{2.2}$$

with

$$F(A) = \int\left(-|A|^2 + \left|\frac{\partial A}{\partial x} - i\frac{\partial^2 A}{\partial y^2}\right|^2 + \tfrac{1}{2}|A|^4\right)dx\,dy. \tag{2.3}$$

In the functional derivative in (2.2), A and A^* are considered independent variables.

Equation (2.1) was again time stepped with the usual pseudospectral scheme. The gradients were computed in Fourier space by multiplying by the wave vector, and the cubic term was assembled in real space. The time stepping was fully implicit with respect to the linear terms. We ran (2.1) for $\epsilon \lesssim 1$ and in boxes that contained as few as four roll pairs. It was then necessary to use up to eight Fourier modes per roll pair to quantitatively simulate the motion of a dislocation, yet all of the spectral weight was in modes with $q \lesssim q_0/2$. As always, the requisite resolution was established by continually increasing it until no further changes occurred. We suspect that most of the modes beyond $q_0/2$ were not required to resolve the defect but to control aliasing in the cubic term.

The parameter space we have to explore has axes corresponding to $\epsilon = (R - R_c)/R_c$, P and geometry which includes both the box size and initial conditions. The dimensions of the periodic box will be denoted by L_x and L_y and the rolls will always lie parallel to the y axis. When used as input to (2.1), the dimensions of the box become $L_x/\xi_{\parallel}$ and $L_y/\xi_{\perp}$. Initially, an extra roll pair segment is introduced into the center of a box already containing n roll pairs. Since the pair of defects will move so as to either lengthen or shorten the added segment, we can characterize our runs as $n+1 \to n$ or $n \to n+1$. The last parameter we will need to introduce and the one most relevant to describing defect motion is the wave vector q of the rolls. It can logically be defined in the presence of a defect as either $2\pi n/L_x$ or $2\pi(n+1)/L_x$, although we will find that the second definition better reduces a variety of different runs to a common form. The conducting state first becomes unstable at $q = q_0 = \pi/\sqrt{2}$ for free-slip boundaries. The corresponding wavelength is $\lambda_0 = 2\pi/q_0$.

Near onset, for $P \gg 1$ the range of q for which stable convection persists is limited to $q^2 - q_0^2 \lesssim q_0^2\epsilon^{1/2}$ by the Eckhaus instability and to $q \gtrsim q_0$ by the zigzag instability.[4] The cross roll instability actually occurs somewhat before Eckhaus in the Boussinesq equations but is absent from (2.1) since we have not allowed for a second amplitude in the perpendicular direction.[4] Since q is quantized in units of $2\pi/L_x$, in order to vary q appreciably in a given box, ϵ can not be made too small. In fact, just to insist that convection with both n and $n+1$ rolls in a particular box is stable, sets a lower bound on ϵ.

The Boussinesq code was initialized with zero velocity and a temperature field proportional to $\cos(qx)\sin(\pi z)$ where q was a multiple of $2\pi/L_x$ that varied with y so as to introduce the desired number of rolls. For Eq. (2.1) we simply set A proportional to $e^{i(q-q_0)x}$ in appropriate units initially. A single dislocation does not give rise to a naturally periodic flow in the y direction. To avoid any question of convergence in the Fourier series, we always worked with pairs of dislocations arranged vertically so that the flow was symmetric under reflection in the line $y = L_y/2$. Irrespective of whatever secondary instabilities occur at later times, the velocity and temperature fields invariably settled down on times of order d^2/κ to the patterns shown in Fig. 1 in the neighborhood of the core. In a larger box, the contours of ω_z would be somewhat more extended laterally but the temperature and horizontal vorticity fields would be indistinguishable.

Several comments on the graphical output are in order. For all $P \gtrsim 20$ and $\epsilon \lesssim 2$, while the dislocation remained reasonably well formed, in excess of 99% of the kinetic energy resided in

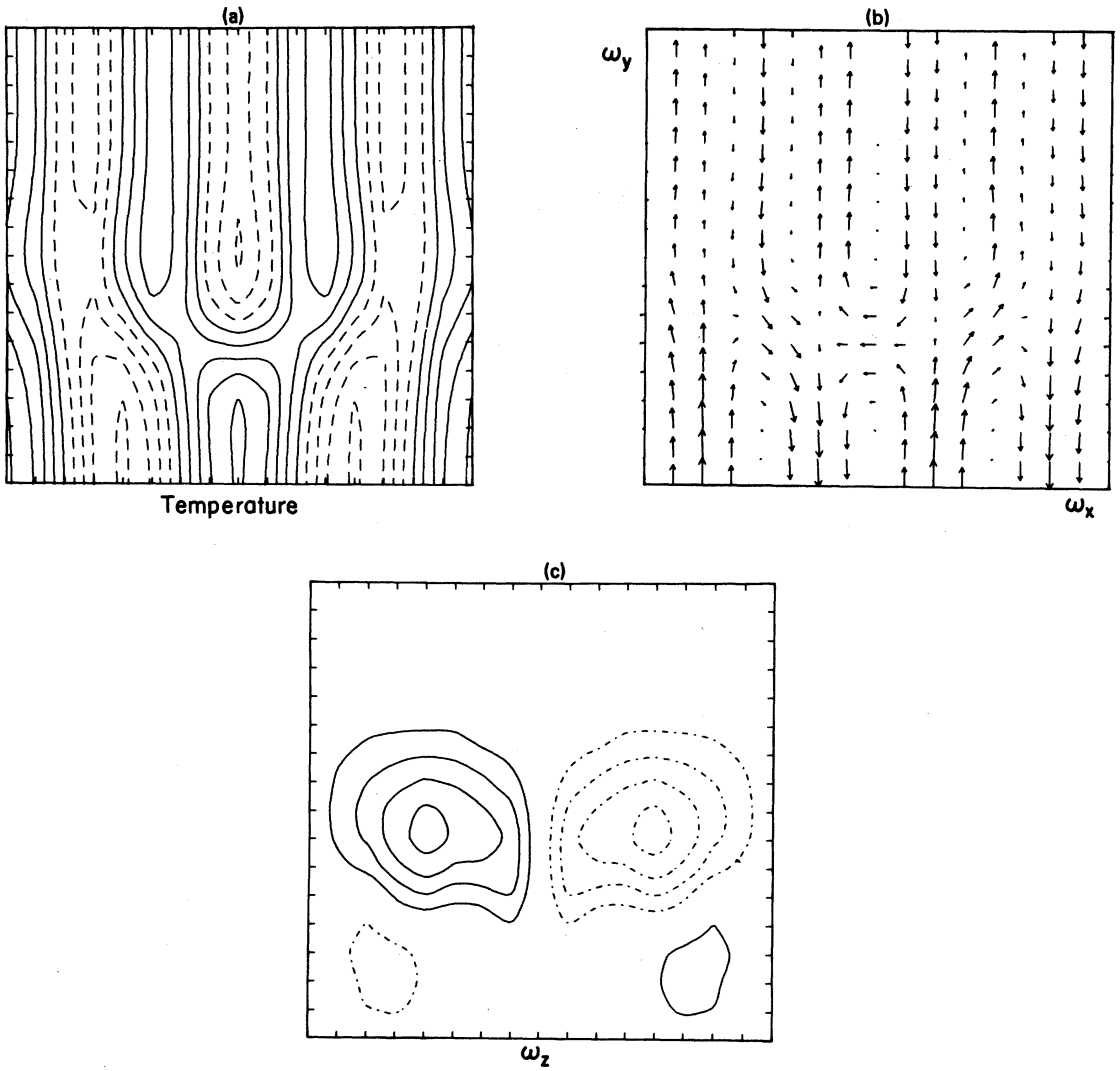

FIG. 1. (a)–(c) A solution to the Boussinesq equations for free-slip boundary conditions in the neighborhood of a defect after the initial conditions have relaxed. Periodic boundary conditions are assumed laterally and only the lower half of the flow field is shown. Horizontal sections were taken for $z=0.5$. The vectors in the second figure indicate, to scale, the magnitude and direction of the horizontal vorticity ω_x, ω_y. The contour lines in the remaining figures are equally spaced with negative regions indicated by dashes. Except for changes in scale, these figures are insensitive to the values of P, ϵ, and q provided one remains within the stable region.

the modes with z dependence $\sim\sin(\pi z)$ or $\cos(\pi z)$ and with a horizontal wave number between $2\pi n/L_x$ and $2\pi(n+1)/L_x$. Similarly, 98% of the temperature variance was either in the above modes or the laterally uniform mode proportional to $\sin(2\pi z)$.

A plot of the temperature field for $z=0.5$ eliminates the uniform mode, that is responsible for the heat transport, and picks up the remaining modes that are closely correlated near onset to the kinetic degrees of freedom. We have found it most advantageous to display these in terms of the horizontal components of the vorticity, since in the absence of a defect, the vorticity is parallel to the y axis. The vertical vorticity is almost entirely concentrated in modes with no dependence on z which is, of course, a particularity of the free-slip boundary conditions.

Even for the parameters for which the dislocation is at least quasistable and ω_z is largest, $\epsilon=2.0$ and $P=20$, one finds $\langle\omega_z^2\rangle/\langle\omega_x^2\rangle \lesssim 0.01$. For $P=100$ and $\epsilon=0.5$, the same ratio is $\sim 3\times 10^{-5}$. Although the averages, denoted by brackets in the preceding line, are taken over the entire fluid, ω_x and ω_z are only nonzero near the defect. Thus the most pronounced effect of the defect on the

velocity field is to bend ω_y into a horseshoe wrapping around the added roll pair (Fig. 1). Although ω_z is small, for $P \sim 20$ an estimate of the integral of ω_z from 0 to $L_x/2$ at a value of y where ω_z is most intense yields a result of order the defect's velocity. If we had simulated the Boussinesq equations with rigid top and bottom surfaces we would expect only ω_z to change significantly. For infinite P, simulations with rigid or free-slip boundaries should be quite similar near onset.

As a rule, we plotted only the temperature field in order to monitor where the defect was and whether any secondary instabilities had occurred in the rest of the fluid. The vorticity fields always bore the same relation to the temperature as in Fig. 1 and moved without distortion along with the dislocation. The overall magnitude of ω_z tended to zero with P^{-1}. Only one type of "core" structure was encountered in all of our runs. In convection, in contrast to many condensed-matter physics problems, it is not at all obvious that only information on some distant closed loop, encircling a defect is sufficient to specify the resulting motions. In a fluid, we could conceive of different core structures giving rise to qualitatively different dynamics.

For $\epsilon = 0.5$, $P = 2$ and by inference any smaller P, we were unable to capture a stable defect for any one of a range of values of q that bracketed

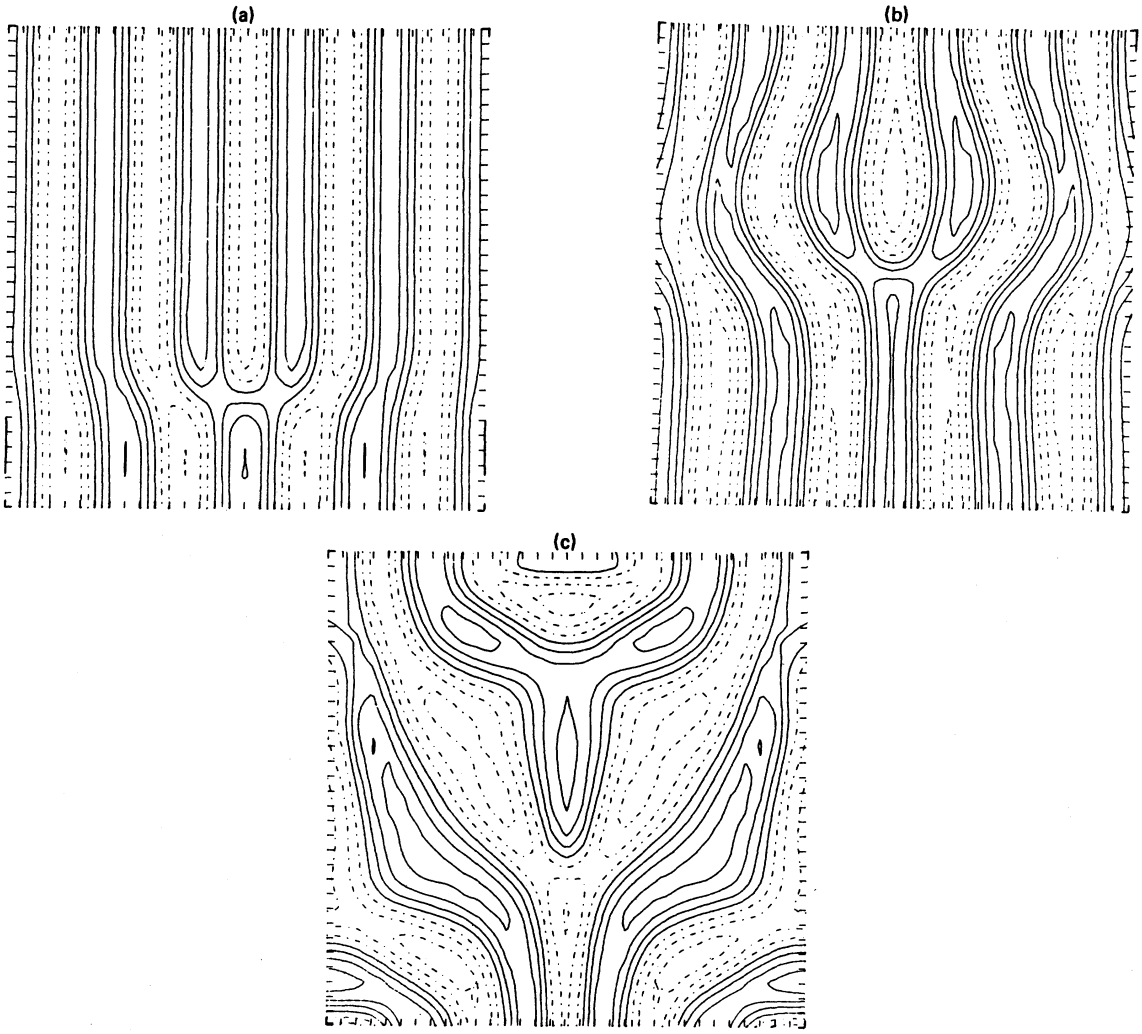

FIG. 2. (a)–(c) Contour plots of the temperature for $\epsilon = 0.5$, $P = 2.0$, and $L_x = L_y/2 = 8\sqrt{2} = 4\lambda_0$ prepared in the same manner as Fig. 1. The successive figures are taken at times of 0.5, 2.0, and 3.5 (with $\kappa = d = 1$) after the temperature was initialized as described in the text. They show the development of a shear induced instability caused by the extra roll. Note that in the last figure, the mean wavelength is somewhat larger than λ_0.

q_0. Figure 2 is indicative of what happened. The initial defect broke down so rapidly that it was felt impossible to suppress the instability by going to smaller ϵ and yet remain within a box of reasonable size. A number of runs were then made with the same parameters for various values of q but with an ordered planform in order to check stability. By comparison with the earlier runs, in which an additional roll was introduced into a periodic field of n others, either $q=2\pi n/L_x$ or $q=2\pi(n+1)/L_x$ appeared unstable if only weakly. There is thus no evidence for these parameters that the dislocation triggered a finite amplitude instability that was otherwise inaccessible. The instability appeared first at long wavelengths in the y direction. Since we were well away from where the well-known high P secondary instabilities occur, we infer that the threshold for either the skewed varicose or oscillatory instability was exceeded.[12,13] Unfortunately, the only analytic results that we are aware of for this shear instability under free-slip boundary conditions are strictly valid only for $P \ll 1$.[12]

For $P = 20$, $\epsilon = 0.5$, $L_x = L_y/2 = 8\sqrt{2}$ (i.e., $4\lambda_0$) and $5 \rightarrow 4$ rolls, the shear instability was largely suppressed. The two defects moved symmetrically parallel to the y axis toward $y = L_y/2$ with nearly uniform velocities. Instead of annihilating at the center, they stopped and two new defects of opposite sign (i.e., a roll was eliminiated) were created along the $x=0$, or L_x line. They then moved toward $y=0$ and L_y. The later stages of a run with the same ϵ, P, but $L_y = L_x = 16\sqrt{2}$ and $9 \rightarrow 8$ rolls are shown in Fig. 3. It is

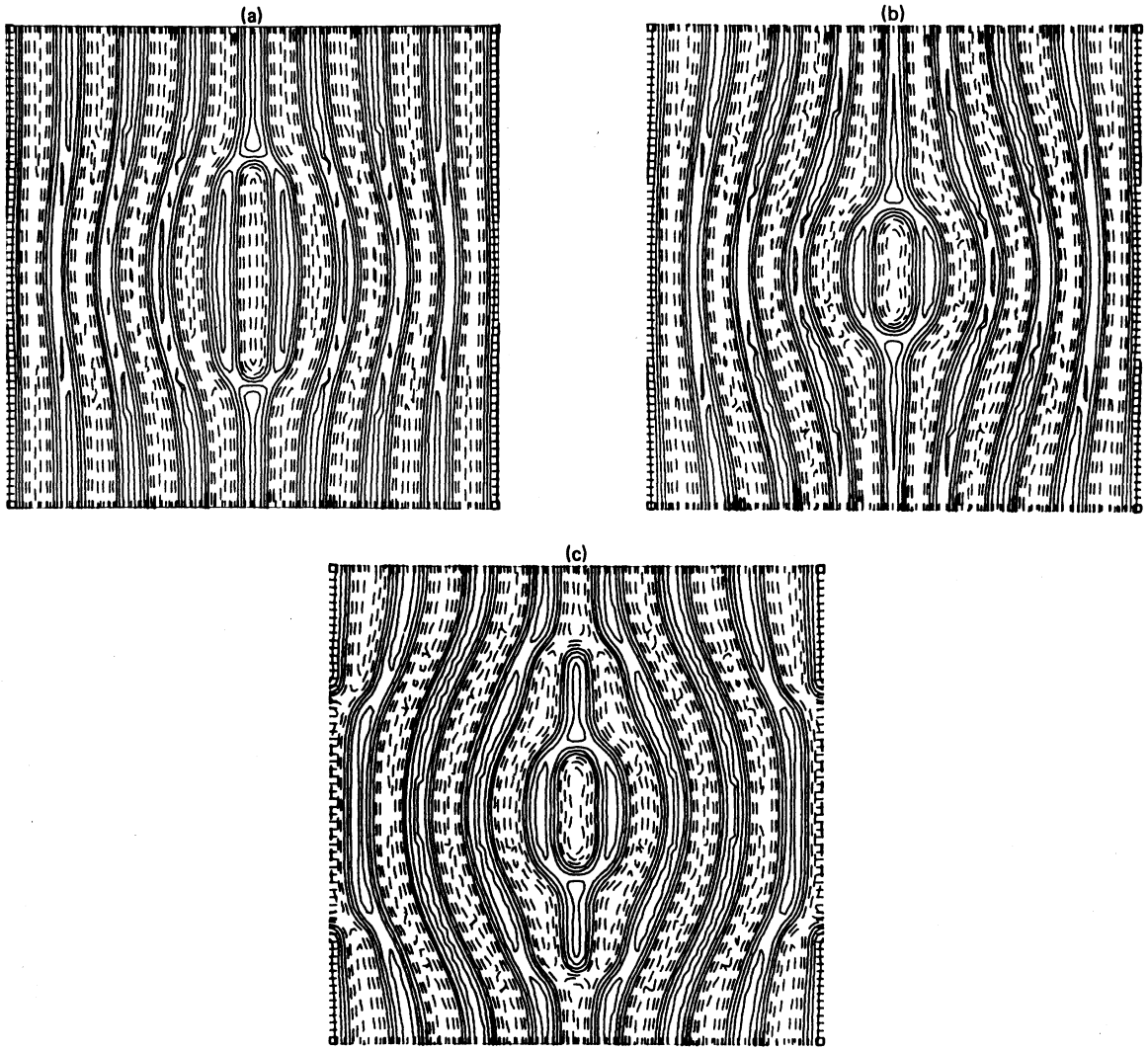

FIG. 3. (a)–(c) Contour plots of the temperature for $\epsilon = 0.5$, $P = 20$, $L_x = L_y = 8\lambda_0$ and at times of 5.0, 10.9, and 17.8. The instability appears qualitatively similar to Fig. 2 but takes much longer to develop.

TABLE II. The Prandtl number dependence of the defect velocity for $L_x = L_y/2 = 4\lambda_0$. An extra roll segment was introduced into a background of 4 rolls at $q = q_0$. The Rayleigh number corresponded to $\epsilon = 0.5$ except for the two bracketed velocities under $P = 100$ and ∞ that were determined for $\epsilon = 1.0$ and 2.0, respectively.

Prandtl No.	20	40	60	100	∞
Velocity	0.90	0.67	0.60	0.57	0.52
				(0.73, 1.20)	(0.57, 0.82)

a bit difficult to imagine a shear instability occurring for these parameters but clearly the presence of the defect led to a breakdown of the pattern. A second run at $P = 20$ and $\epsilon = 2$ broke down in a manner similar to Fig. 2 at $P = 2$, $\epsilon = 0.5$.

A Prandtl number of 40 was the first in which for $\epsilon = 0.5$. $L_x = L_y/2 = 8\sqrt{2}$ and $n = 4$, a defect pair proceeded all the way to $y = L_y/2$ and annihilated without exciting any secondary instabilities. However, when the same flow pattern with a single defect pair was rerun in a larger box, $L_x = 48\sqrt{2}$ and $L_y = 24\sqrt{2}$, a transverse undulation at a wavevector of $2\pi/L_y$ developed in the rolls well away from the defect. The velocity of the defect was distinctly nonuniform.

In Table II we collect data on the Prandtl number dependence of the velocity for a fixed, though relatively small box. After an initial transient, the velocity was constant to within about 5%, although there was a small negative acceleration that became more pronounced near $y = L_y/2$. Once initial transients had relaxed and prior to annihilation, the velocity and temperature fields in the neighborhood of either defect invariably assumed the form $f(x, y-vt)$ provided no secondary instabilities occurred. Comparative velocity data were extracted for similar ranges of y.

The existence of appreciable defect motion at $P = \infty$ clearly rules out any explanation based solely on the nonlinear terms in the Navier-Stokes equation or the existence of a vertical vorticity. The remaining runs were designed to clarify the dependence of v on geometry and ϵ, and were performed at infinite Prandtl number both because of the considerable economies in computer time thereby obtained, and the enhanced range of Rayleigh numbers that could be explored without interference from secondary instabilities. On the most naive level, however, the vertical vorticity could account for the difference between the $P = 20$ and $P = \infty$ entries in Table II. The amplitude equation only predicts a 5% variation in velocity over this range of P (Table I). The velocities at $\epsilon = 1.0$ and 2.0 at $P = 100$ and ∞ suggest that the approach to the infinite Prandtl number limit may not be uniform in ϵ.

TABLE III. The velocity of a defect in physical units obtained from a numerical integration of the Boussinesq equations and the amplitude equations (2.1) as a function of reduced Rayleigh number ϵ, the number of rolls in the undisturbed pattern n, and their wavenumber q. The periodic computational box had lateral dimensions of $L_x = 2\pi n/q$ and $L_y = 2L_x$ for $n \leq 6$, $L_y = L_x$ for $n = 12$, and $L_y = L_x/2$ for $n \geq 24$.

Velocity				
Boussinesq	Eq. (2.1)	ϵ	n	q
0.48	0.70	0.2	4	q_0
0.52	0.64	0.5	4	q_0
0.57	0.57	1.0	4	q_0
0.82		2.0	4	q_0
1.01		4.0	4	q_0
0.29	0.35	0.2	6	q_0
0.29	0.30	0.5	6	q_0
0.39	0.28	1.0	6	q_0
0.81		2.0	6	q_0
0.10	0.10	0.2	12	q_0
0.12	0.093	0.5	12	q_0
0.22	0.086	1.0	12	q_0
0.79		2.0	12	q_0
0.06	$\lesssim$0.04	0.5	24	q_0
0.63		0.25	12	$\frac{15}{13} q_0$
0.63		0.5	12	$\frac{15}{13} q_0$
0.71		1.0	12	$\frac{15}{13} q_0$
0.91		0.5	12	$\frac{16}{13} q_0$
0.49		0.5	24	$\frac{15}{13} q_0$
0.26	0.23	0.5	26	$\frac{13}{12} q_0$

The dependence of the velocity on q was largely explored at $\epsilon = 0.5$ which was a compromise between the competing requirements of proximity to onset and freedom from secondary instabilities for as wide a range of q as possible (Table III). When one scans the data for $n \to n+1$ rolls with $L_x = 2\pi n/q_0$, the velocity clearly tends to zero as n increases; although from the complete numerical data, it was apparent that the initial relaxation time before a constant velocity was achieved also grew. To see when the defect velocity would change sign, a number of runs were made with the $7 \rightharpoonup 6$ roll pattern for $L_x/\lambda_0 = 6.0$, 6.5, and 7.0. The defect reversed direction between the last two runs but its velocity was by no means constant.

The next set of entries in Table III shows that the velocity in a small box can be mimicked by compressing an infinite system, i.e., letting $2\pi n/L_x$ exceed q_0. A bit of calculation shows that the best way to collapse data for different boxes and compressions is to work in terms of the wave number defined with the defect present, i.e., $q = 2\pi(n+1)/L_x$.

Our analytic theory is confined to a solution of the amplitude equations (2.1) in the limit of a large box, small compression, and $\epsilon \to 0$. Since it is virtually impossible to convincingly simulate the Boussinesq equations in this limit, our numerical solutions of (2.1) serve as a bridge between the simulations and what can be done analytically. We can then make comparisons between simulations in the same box with the knowledge that the geometry is treated correctly and, in addition, compare the initial transients which are difficult to calculate analytically. It is of some importance to establish that the lowest-order amplitude equations quantitatively describe dislocation motion even if they could not be treated analytically.

To set the scale for what can be expected quantitatively from Eq. (2.1), it is useful to cite in physical units the values it gives with an ideal pattern for the Nusselt number, $N = 1 + 2\epsilon$, the mean-square vorticity along the roll axis $\langle \omega_y^2 \rangle = \frac{27}{2}\pi^4\epsilon$, and the ratio of the mean-square temperature in the fundamental mode to $\langle \omega_y^2 \rangle$, $9\pi^2/2$. The correct numbers are 1.33, 272.0, and 44.4 for $\epsilon = 0.2$, and 1.67, 712.0, and 44.4 for $\epsilon = 0.5$. One does quite well on the vorticity or velocity but rather poorly on the Nusselt number, especially since one should compare $N - 1$.

The defect position as a function of time is shown in Fig. 4 for $\epsilon = 0.5$ and $13 \to 12$ rolls. For $t \lesssim 1$, the two codes gave quite different results since they were initialized differently. The deaccelerating motion for $2 \lesssim t \lesssim 7$ looks quite similar in that a shift of $y(0)$ and a change in scale would bring the curves into coincidence. The velocity is effectively constant in both cases for $t > 7$, and it is these numbers that appear in Table III. For the more compressed systems such as $5 \to 4$ rolls, the velocity is constant for $t \gtrsim 2$.

When the entries in Table III are inspected, the accuracy of Eq. (2.1) obviously improves as L_x increases for small ϵ. The agreement at $\epsilon = 1.0$ for $5 \to 4$ rolls is obviously fortuitous. Any of the discrepancies in Table III could be rationalized, it appears, by supposing that higher-order terms in ϵ modify the coefficients in Eq. (2.1) yet preserve the feature that it is derivable from a potential. More elaborate expansions would be justified in our view only if there was clear evidence that the motion was not relaxational in the sense of Eqs. (2.2) and (2.3).

III. ANALYTIC SOLUTION OF THE AMPLITUDE EQUATION

The numerical simulations in the preceding section brought to light two qualitative features of a

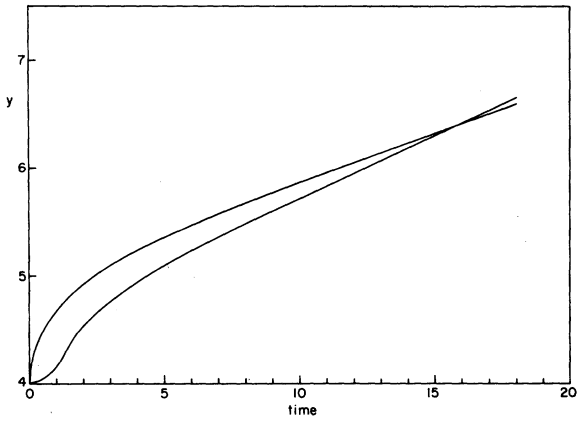

FIG. 4. Plot of position y vs time for the lower of a pair of defects placed in a box with $\epsilon = 0.5$, $P_r = \infty$, and $L_x = L_y = 24\sqrt{2} = 12\lambda_0$. The pattern into which the additional roll was introduced contained 12 rolls across, i.e., $q = q_0$. The upper curve is from a numerical solution of the amplitude equation (2.1) and the lower one was derived from the Boussinesq equations.

dislocation's motion that merit explanation; namely, that the velocity is nearly constant and independent of ϵ for $\epsilon \lesssim 1$. The former property might suggest that the dynamics is generated locally, i.e., in the core region and is independent of any "interaction" the defect might have with its counterpart within the box or their images created by the periodic boundary conditions. The insensitivity to ϵ is surprising since one expects all motions to become more sluggish as $\epsilon \to 0$.

Let us assume that the lowest-order amplitude equation correctly describes a defect near onset and imagine working in an infinite system with some compression $\delta q = q - q_0 > 0$. (A negative compression $\delta q < 0$ for $P \gg 1$ leads to an instability of the basic roll pattern.) Actually if ϵ and δq are the only parameters to enter the amplitude equation, and if the defect velocity v is independent of ϵ, v must vary as $\delta q^{3/2}$. In this section we will demonstrate this relationship, and show under what circumstances the interaction with other defects and walls is indeed negligible. Within a linearized theory we will calculate the numerical value of v and the envelope of the perturbed flow field around the defect.

The nature of the mathematical problem we face is to go from a nonlinear field theory, which in principle contains everything known about the dynamics outside of the core region, to equations of motion for the point defects. In other situations where this type of problem arises, such as in the representation of the two-dimensional Euler equations by point vortices, the equation of motion for the points follows from their convection by the local velocity field. In crystals

where dislocation motion is of some technical importance, the applicable theory assumes relaxational motion in response to an elastic strain energy.[8] The closest analog to our problem, and one that has not been addressed to the best of our knowledge, arises in magnetic systems where the dynamics of the local spin density is known at the level of mode coupling. One could then ask from this field theory, how do topological singularities in the spin configuration move about.

In analogy to our numerical work, let us specialize to the case of two defects at $x=0$, $y=y_\pm$ in an infinite compressed roll pattern. When $\delta q>0$, they will move toward each other with velocities $\partial y_\pm/\partial t=\mp v$. The second defect is more a convenience than a necessity, and a distant wall would serve equally well. Our initial configuration could be created by inserting an extra roll pair of length y_+-y_- into an ordered array. To simplify the analysis we will assume $\delta q \ll 1$ and $\delta q^{-1/2} \ll y_+-y_-$. We will work in the dimensionless scaled units of (2.1) until a final form for v is obtained, whereupon the dimensional scales appropriate to rigid or free-slip boundary conditions from Table I will be restored [see (3.11b)].

Our solution proceeds in two steps. We first find the perturbed flow field around a defect retaining v as a parameter and then determine v from the formally exact equation:

$$\int \left|\frac{\partial A}{\partial t}\right|^2 dx\,dy = -\frac{1}{2}\frac{\partial F}{\partial t}, \tag{3.1}$$

where $A(x,y,t)$ is a solution to (2.1) and F is the numerical value of the functional in (2.3) evaluated for $A=A(x,y,t)$. If F were interpreted as twice an energy, then (3.1) simply says that for overdamped motion, the rate of energy dissipation equals the rate of decrease of potential energy. If, furthermore, F depends on t only through y_+-y_-, then $\partial F/\partial t=-2v\partial F/\partial(y_+-y_-)$ ($v>0$) which is merely the statement that power equals force times velocity.

Since Eq. (2.1) is relaxational in character, it is natural to suppose that if v could be made small enough, the surfaces of constant F in function space would contain a pronounced valley with a gently sloping floor. The position of the defect parameterizes points along the valley and as $v\to 0$, all other degrees of freedom relax to values conditioned by the presence of a stationary defect. Elements of this picture will emerge in the analysis to follow.

In the absence of defects, the stationary solution of Eq. (2.1) is $A_0=(1-\delta q^2)^{1/2}e^{i\delta q x}$. When a dislocation is present we set $A=A_0e^{i\Theta(x,y,t)}[1+u(x,y,t)]$, where Θ and u are real fields. We assume that $\nabla\Theta$ and u are small sufficiently far from the defect and linearize Eq. (2.1) around A_0:

$$\frac{\partial u}{\partial t}=-2(1-\delta q^2)u-2\delta q\frac{\partial\Theta}{\partial x}+T_{\rm NL}, \tag{3.2a}$$

$$\frac{\partial\Theta}{\partial t}=2\delta q\frac{\partial u}{\partial x}+\frac{\partial^2\Theta}{\partial x^2}+2\delta q\frac{\partial^2\Theta}{\partial y^2}-\frac{\partial^4\Theta}{\partial y^4}+T_{\rm NL}. \tag{3.2b}$$

A number of higher-order gradients that will be irrelevant to the linearized analysis for $\delta q\to 0$ were omitted in (3.2a) and (3.2b). The nonlinear terms in $\nabla\Theta$, $T_{\rm NL}$, will be discussed below.

While A must be single valued throughout space, Θ need not be; and $\int_A^B(\vec{\nabla}\Theta)\cdot d\vec{l}$ counts the number of rolls traversed on a path from A to B, reckoned with respect to the compressed background. Thus, for a path encircling either of the defects at $y_\pm$ one finds, respectively,

$$\oint \vec{\nabla}\Theta\cdot d\vec{l}=\pm 2\pi, \tag{3.3}$$

implying that an extra roll pair was inserted between $y=y_\pm$. To work with a single-valued function Θ it is convenient to introduce a branch cut along $y_-\le y\le y_+$, $x=0$. The function Θ exhibits a jump discontinuity of size 2π across the cut.

In the limit $\delta q\to 0$ the coupling to u in (3.2b) which gives rise to the Eckhaus instability for $1-3\delta q^2=0$ may be omitted.[4] We have finally

$$\frac{\partial\Theta}{\partial t}=\frac{\partial^2\Theta}{\partial x^2}+2\delta q\frac{\partial^2\Theta}{\partial y^2}-\frac{\partial^4\Theta}{\partial y^4}-2\pi\frac{\partial\delta(x)}{\partial x}[\eta(y-y_+)-\eta(y-y_-)]. \tag{3.4}$$

The singular term involving the step function η, $[\eta(y<0)=0,\ \eta(y>0)=1]$ was inserted to make Θ single valued and facilitate the use of Fourier transforms. Equation (3.4) clearly is the superposition of contributions from two defects with opposite signs at $y=y_\pm$.

It will be useful in what follows to display the static deformation $\Theta(x,y)$ due to a single defect at $x=y=0$ obtained by setting $\partial\Theta/\partial t=0$ in (3.4). For $y\gg\delta q^{-1/2}$ or $x\gg\delta q^{-1}$,

$$\Theta=\tan^{-1}\left(\frac{y}{\sqrt{2\delta q}x}\right), \tag{3.5a}$$

i.e., Θ is just the angle itself measured in scaled units. In the other limit,

$$\Theta=\frac{\pi}{2}\,\mathrm{sgn}(x)\left[\mathrm{erf}\left(\frac{y}{\sqrt{4|x|}}\right)+1\right]. \tag{3.5b}$$

We shall refer to the first regime as the $x-y$ limit and to Eq. (3.5b) as the smectic limit. The crossover between these two regimes is illus-

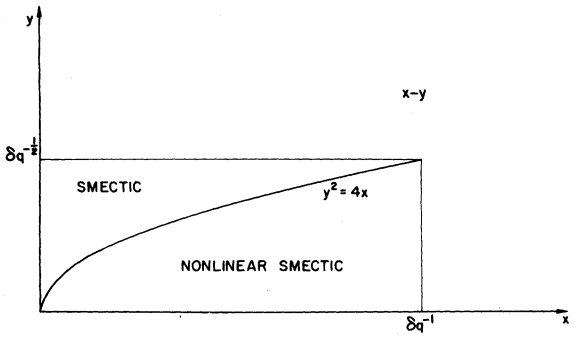

FIG. 5. An illustration of the x-y and smectic domains for the envelope of flow field around a defect at $x=y=0$. Nonlinear terms cannot be neglected near either of the crossover lines, $y\sqrt{\delta q}\sim 1$ or $x\delta q\sim 1$. In addition, nonlinear terms are important below the parabola, $y^2=4x$, for $1\ll x\ll \delta q^{-1}$.

trated in Fig. 5.

Equation (3.4) can be solved in a number of ways; in particular, one can invert the homogeneous part of the equation onto the inhomogeneous term and express Θ as an integral over $y_\pm$ at earlier times. For our purposes, it will be easier to assume $y_\pm(t)$ is linear in t and examine the validity of this ansatz later,

$$y_\pm(t)=\pm y_0 \mp vt\,. \tag{3.6}$$

Equations (3.4) and (3.6) then allow for solutions, which can be written as the superposition of contributions from two defects, each depending on time only through $y_\pm(t)$, i.e.,

$$\Theta(x,y,t)=f^+(x,y-y_+(t))+f^-(x,y-y_-(t)), \tag{3.7a}$$

with

$$f^+(x,y)=f^-(x,-y)\,. \tag{3.7b}$$

Equation (3.4) may then be rescaled so as to eliminate δq, i.e., let $x\to x/\delta q$, $y\to y/\delta q^{1/2}$, and $t\to t/\delta q^2$, whereupon we find that v only occurs in the combination $v/\delta q^{3/2}$. This reduction continues to hold in the presence of nonlinear terms in $\nabla\Theta$ as is apparent from the form of the gradients in (2.3).

The left-hand side of (3.1) is most easily derived from (3.4) by Fourier transforming in both space and time. One finds,

$$\int_{-\infty}^{\infty}\left|\frac{\partial A}{\partial t}\right|^2 dx\,dy=\int_{-\infty}^{\infty}\left(\frac{\partial\Theta}{\partial t}\right)^2 dx\,dy \tag{3.8a}$$

$$=2v^2\int_{-\infty}^{\infty}\frac{k^2\,dk\,dp}{(k^2+2\delta q p^2+p^4)^2+v^2p^2}$$

$$=\frac{2v^2}{\sqrt{2\delta q}}\int_{-\infty}^{\infty}\frac{k^2\,dk\,dp}{(k^2+p^2+p^4)^2+v^2p^2/(8\delta q^3)}. \tag{3.8b}$$

The term arising from $\int(\partial u/\partial t)^2$, as well as the higher gradients that were omitted from (3.4) are of higher order in δq than the terms we retained in (3.8). Note that for $\delta q\to 0$, the integral in (3.6) is naturally limited to wave numbers $\ll q_0$, so that the amplitude equations should apply quantitatively throughout the range of integration. Retention of the fourth-order derivative $\partial^4/\partial y^4$, in (3.2b) was necessary to guarantee the convergence of (3.8b) for large momenta. Similarly, if v were set to zero in (3.8b), the integral would diverge at long wavelengths. This divergence is in part a manifestation of the diffusive form of Eq. (2.1), which implies that no matter how slowly the defect moves, there will always be slower modes present in the surrounding medium at long wavelengths.

To the same order as (3.4), F becomes

$$\frac{1}{2}F=\int\left[\delta q\frac{\partial\Theta}{\partial x}+\delta q\left(\frac{\partial\Theta}{\partial y}\right)^2+\frac{1}{2}\left(\frac{\partial\Theta}{\partial x}\right)^2+\frac{1}{2}\left(\frac{\partial^2\Theta}{\partial y^2}\right)^2\right]dx\,dy \tag{3.9a}$$

and

$$-\frac{1}{2}\frac{\partial F}{\partial t}=4\pi\delta q v-2v\,\frac{\partial U(y_+-y_-)}{\partial(y_+-y_-)}\,. \tag{3.9b}$$

The linear term, proportional to δq in (3.9b) is analogous to what one would find in an elastic solid under a positive external pressure if an extra row of atoms was inserted. It arises because $\partial\Theta/\partial x$ is singular at $x=0$ for $y_-\le y\le y_+$, i.e., $\partial\Theta/\partial x=2\pi\delta(x)[\eta(y-y_+)-\eta(y-y_-)]$. (Alternatively, one could dispense with the singularity by introducing a branch cut between $y=y_\pm$ to keep Θ single valued. The contribution to F is of course unchanged.) The potential U in (3.9b) arises from the quadratic terms in (3.9a) and will be displayed below. The defect's velocity v is not constant only when the potential term is comparable to the first term in (3.9b) which in practice means $(y_+-y_-)\delta q^{1/2}\sim 1$. During most of our simulations, and certainly whenever we extracted a velocity, the potential term in (3.9b) was no more than 5–10% of the total.

If U can be neglected, if follows from (3.1) (3.8b), and (3.9b) that $\alpha=v^2/(8\delta q^3)$ satisfies the equation

$$\sqrt{\alpha/2}\int_{-\infty}^{\infty}\frac{dp}{\{p^2+\alpha p^4+[p^2+(p^2+\alpha p^4)^2]^{1/2}\}^{1/2}}=1\,, \tag{3.10}$$

or

$$v=\beta\delta q^{3/2}\,;$$

$$\beta=1.47\,. \tag{3.11a}$$

The value of β given in (3.11a) was derived from (3.10) and is distinctly different from $\beta = 0.84$ found from the numerical solutions of (2.1). In physical units, $\kappa = d = 1$, we then find from Table I for either free-slip or rigid boundaries

$$v = \beta \xi_{\parallel}^2 \delta q^{3/2} / (\sqrt{2 q_0} \tau) . \tag{3.11b}$$

Note that v is positive in (3.11b), i.e., $\delta q > 0$ and the defects approach each other. In addition, the dependence of the length and time scale factors on ϵ cancels in (3.11b). The best fit of β to the simulations of (2.1) will be discussed below, but is listed below (3.11a) for completeness.

It follows from Eq. (3.10) and the scaling, $v \sim \delta q^{3/2}$ in (3.11a), that it is not possible to eliminate v from (3.8b) or in fact treat the corrections to the static solution perturbatively by letting $\delta q \to 0$.

Within the linearized theory defined by (3.4), it is of some interest to explicitly calculate $\Theta(x, y, t)$ and hence the envelope function $A = (1 - \delta q^2)^{1/2} e^{i \delta q x} e^{i \Theta}$ for a single defect in isolation or about either member of the pair considered above, provided $(y_+ - y_-) \delta q^{1/2} \gg 1$. With a suitable choice of origin and assuming an extra roll was inserted along $y > 0$ at $t = 0$, we can write $\Theta(x, y, t) = f^-(x, y - vt)$, with $v > 0$ (3.7). It is then convenient to define $\tilde{x} = 2 \delta q x$, $\tilde{y} = \sqrt{2 \delta q}(y - vt)$, and $v = (2 \delta q)^{3/2} \sqrt{\alpha}$ and to calculate

$$I(\tilde{x}, \tilde{y}) = \int_{-\infty}^{\infty} \frac{dp\, dk}{2\pi} \frac{e^{ik\tilde{x} + ip\tilde{y}}}{k^2 + p^2 + p^4 - ip\sqrt{\alpha}} , \tag{3.12a}$$

where

$$\frac{\partial f^-}{\partial \tilde{y}} = \frac{\partial I}{\partial \tilde{x}} . \tag{3.12b}$$

We again note that δq does not appear in (3.12a) and there is no physically reasonable way to remove v from the envelope f since $\alpha = \beta^2/8$ is a numerical constant, (3.11a).

When $\tilde{x}, \tilde{y} \ll 1$ or $k, p \gg 1$, it is clear from (3.12) that derivatives of Θ revert to the smectic solution (3.5) with the substitution $y \to y - vt$. The envelope is, however, sensibly different from the static solution in the long-wavelength or $x - y$ limit. When either $\tilde{x} \gg 1$ or $\tilde{y} \gg 1$ it is possible to drop p^4 from the denominator of (3.12a) and rewrite I in either of the following two equivalent forms,

$$I = \tfrac{1}{2} e^{-\tilde{y}\sqrt{\alpha}/2} \int_{-\infty}^{\infty} \frac{\exp[-|\tilde{y}|(k^2 + \alpha/4)^{1/2}]}{(k^2 + \alpha/4)^{1/2}} e^{ik\tilde{x}} dk , \tag{3.13a}$$

$$I = \exp[-(\tilde{y} + |\tilde{x}|)\sqrt{\alpha}/2] \times \int_0^{\infty} e^{-|\tilde{x}|\lambda} \frac{\sin[|\tilde{y}|(\lambda^2 + \sqrt{\alpha}\lambda)^{1/2}]}{(\lambda^2 + \sqrt{\alpha}\lambda)^{1/2}} d\lambda , \tag{3.13b}$$

which facilitate the development of asymptotic expansions.

For $|\tilde{x}| \ll |\tilde{y}|$ one finds

$$\frac{\partial I}{\partial \tilde{x}} = -\tfrac{1}{2} \pi^{1/2} \alpha^{1/4} \tilde{x} \tilde{y}^{-3/2} \exp[-\sqrt{\alpha}(\tilde{y} + |\tilde{y}|)/2] . \tag{3.14}$$

Thus, in the direction the defect is advancing, $\partial I / \partial \tilde{x}$ is exponentially small, whereas it decays algebraically in the region diametrically opposite. Equation (3.14) should be contrasted with the static solution

$$\frac{\partial I}{\partial \tilde{x}} = \frac{-\tilde{x}}{\tilde{x}^2 + \tilde{y}^2} , \tag{3.15}$$

which applies for all $\tilde{x}, \tilde{y} \gg 1$. Ahead of the advancing defect Θ is effectively zero, while behind it is larger than the static solution.

For the calculation of the potential U in Eq. (3.9b) the time-dependent envelope function $\Theta(x, y, t)$ should be used. It is then convenient to perform a partial integration,

$$U = -\tfrac{1}{2} \int d\vec{x} \left[\left(\frac{\partial \Theta}{\partial x} \right)^2 + 2 \delta q \left(\frac{\partial \Theta}{\partial y} \right)^2 + \left(\frac{\partial^2 \Theta}{\partial y^2} \right)^2 \right] , \tag{3.16a}$$

$$= \tfrac{1}{2} \int d\vec{x}\, \Theta \left(\frac{\partial^2}{\partial x^2} + 2 \delta q \frac{\partial^2}{\partial y^2} - \frac{\partial^4}{\partial y^4} \right) \Theta , \tag{3.16b}$$

and use Eq. (3.4) and (3.7) to rewrite U in the following way:

$$U = U_1 + U_2 , \tag{3.17a}$$

$$U_1 = -\tfrac{1}{2} \int d\vec{x} (f^+ + f^-) 2\pi \frac{\partial \delta}{\partial x}(x) \times [\eta(y - y_+(t)) - \eta(y - y_-(t))] , \tag{3.17b}$$

$$U_2 = \tfrac{1}{2} \int d\vec{x} (f^+ + f^-) v \frac{\partial}{\partial y} (f^+ - f^-) . \tag{3.17c}$$

Actually only the derivative $\partial U / \partial (y_+ - y_-)$ is needed for our calculations. The first contribution,

$$\frac{\partial U_1}{(y_+ - y_-)} = \pi \int_{-\infty}^{+\infty} dy \frac{\partial^2}{\partial x \partial y} [f^+ \eta(y - y_-(t)) + f^- \eta(y - y_+(t))] \Big|_{x=0} , \tag{3.18}$$

is negligible in the limit $(y_+ - y_-) \gg \delta q^{-1/2}$, since the integration in Eq. (3.18) covers only those regions

where the envelope $f^-(f^+)$ is reduced by an exponential factor $\exp[-\sqrt{2\alpha\delta q}(y-y_-)]$ for $y>y_-$ ($\exp[-\sqrt{2\alpha\delta q}(y_+-y)]$ for $y<y_+$). Therefore, the second term

$$\frac{\partial U_2}{\partial(y_+-y_-)}=v\int d\vec{x}\left(\frac{\partial f^+}{\partial y}\right)\left(\frac{\partial f^-}{\partial y}\right) \tag{3.19}$$

dominates the potential U. It is easily evaluated in the $x-y$ limit with the result

$$\frac{\partial U}{\partial(y_+-y_-)}\simeq\frac{\partial U_2}{\partial(y_+-y_-)}\simeq-\left(\frac{v\pi^3}{(y_+-y_-)}\right)^{1/2}. \tag{3.20}$$

If instead of the time-dependent envelope function we had used the static solution to calculate the potential, we would have found

$$\frac{\partial U}{\partial(y_+-y_-)}=-2\pi\,\mathrm{Im}\left(\int_0^\infty dp\,\frac{(2\delta q+p^2)p}{(2\delta q p^2+p^4)^{1/2}}e^{ip(y_+-y_-)}\right). \tag{3.21}$$

For $(y_+-y_-)>0$ the contour of integration has to be chosen such that $0<\arg p<\pi/4$. In the x-y limit one recovers from (3.21) the well-known logarithmic interaction, i.e.,

$$\frac{\partial U}{\partial(y_+-y_-)}=-2\pi\sqrt{2\delta q}\,\frac{1}{(y_+-y_-)}. \tag{3.22}$$

As compared with Eq. (3.20), the static interaction falls off more rapidly by a factor $(y_+-y_-)^{1/2}$. In the smectic limit the static potential $U\to 0$. It seems plausible that this result also holds for the potential calculated with the time-dependent envelope, since in the limit $\tilde{x},\tilde{y}\ll 1$ the solution should become independent of $\sqrt{\alpha}$ [see for example, Eq. (3.12a)].

While the linearized equation (3.4) permitted us to arrive at an explicit solution, it is not internally consistent. Among the nonlinear terms omitted from (3.4) are those involving $\nabla\Theta$ in (3.2b),

$$T_{\mathrm{NL}}=2\frac{\partial\Theta}{\partial x}\frac{\partial^2\Theta}{\partial y^2}+4\frac{\partial\Theta}{\partial y}\frac{\partial^2\Theta}{\partial x\partial y}+6\left(\frac{\partial\Theta}{\partial y}\right)^2\frac{\partial^2\Theta}{\partial y^2}+\cdots. \tag{3.23}$$

If we use the linear solution (3.5) to estimate (3.23) in the smectic limit $\tilde{x}\ll 1$, $\tilde{y}^2/\tilde{x}\lesssim 1$, and $x,y\gg 1$, one finds $(\partial\Theta/\partial y)(\partial^2\Theta/\partial x\partial y)$ exceeds the linear terms we retained while $(\partial\Theta/\partial y)^2(\partial^2\Theta/\partial y^2)$ is of the same order. In the x-y limit $\tilde{x},\tilde{y}\gg 1$, the nonlinear terms are indeed smaller than those we retained and (3.12a) stands. For $\tilde{x}\sim 0$, $\tilde{y}<0$, (3.23) is of the same order as the next to leading term in (3.14). When the left-hand side of (3.1) is computed from $\int(\partial\Theta/\partial t)^2\,dx\,dy$, the regions $\tilde{x}\sim 1$ or $\tilde{y}\sim 1$ about each defect dominate the integral and one must suppose that if the correct nonlinear solution were used in place of (3.4), the integral in (3.8b) would change by an amount of order 1. The other side of (3.1) will be unchanged to the extent that F is dominated by the linear term $4\pi\delta q(y_+-y_-)$. The dimensionless factor β in (3.11a) is thus only approximate and not systematic in any small parameter. The scaling of v, contained in (3.10)–(3.11), we again remind the reader, remains unaltered, if nonlinear terms are taken into account.

Our analytic solution is of course only valid in the limit $\delta q\ll 1$ while to compare with any of our numerical simulations, one must also insist that $\delta q\gg 2\pi\xi_{\parallel}/L_x$. The second restriction could be lifted if the analytic theory were redone with periodic boundary conditions in x. This has not been done systematically, though it is plausible that the coefficient of the term in F linear in y_+-y_- will be enhanced when the boundary conditions prevent the roll pattern from relaxing fully in the x direction. It is less obvious how the $\delta q^{1/2}$ factor from (3.8b) is modified by periodic boundary conditions.

We have found empirically that the best fit to the velocity data from the amplitude equation is obtained if we set $\delta q+q_0=2\pi(n+1)/L_x$ in (3.11b). This definition was then used to extract the numerical value of β cited below (3.11a) from the data in Table IV. Even though the largest compressions tabulated there are not much below the cutoff imposed by the Eckhaus instability, the relation $v\sim\delta q^{3/2}$ remains valid.

To summarize then, we have shown that the defect velocity scales as $\delta q^{3/2}$ and is independent of ϵ even when the nonlinear terms in $\nabla\Theta$ are included. Our theory does not rule out a dependence of the velocity, in physical units, on ϵ when δq

TABLE IV. The dependence of the defect velocity, in physical units $\kappa=d=1$, on compression from simulations of the amplitude equation for $\epsilon=0.5$ and $L_x=32\lambda_0$. The wave number of the pattern before the defect is introduced is $nq_0/32$ and $\delta q+q_0=(n+1)q_0/32$. A comparable run with $L_x=12\lambda_0$ and $n+1=13$, 14, 15 gave $v/\delta q^{3/2}=1.13$, 1.60, 1.57.

$n+1$	34	35	36	37	38	39
$v/\delta q^{3/2}$	1.61	1.60	1.61	1.64	1.68	1.72

is not small, for instance near the point of Eckhaus instability, although numerically this did not occur. The key step in the demonstration was the observation that the compressional term in $\partial F/\partial(\gamma_+ - \gamma_-)$ dominated the remaining terms that depended explicitly on the separation. By the same token, interaction effects that would lead to a variable v are small. A correct calculation of the coefficient of proportionality between v and $\delta q^{3/2}$ requires the solution of a nonlinear equation and has not been attempted. In order to compare with laboratory experiments, one should use (3.11b) with the constant β determined numerically from Table IV and the scale factors appropriate to rigid boundaries from Table I.

It is not out of the question that the Prandtl number dependence of v could also be established analytically. By continuing the expansion that gave rise to (2.1), one would eventually find the field ω_z generated by a defect solution to (2.1). Since only one bifurcation has taken place, there can be only one free-envelope function. To understand how ω_z reacts back on the defect of course requires the higher-order corrections to (2.1) which are no longer purely relaxational in character.[14] Clearly, convective effects must enter. There are in fact well-known propagating, solitonlike solutions to the two-dimensional Euler equations consisting of two blobs of vorticity of opposite sign that rather resemble ω_z in Fig. 1.[15] The familiar problem of two-point vortices of opposite sign is simply one limit of these more general finite area vortex solutions. Some way has to be found for a single envelope solution, $A(x, y - vt)$, to decompose v into a convective piece that would follow from ω_z and the potential contribution (3.11) that has already been found.

IV. CONCLUSION

Our numerical experiments and theory leave one with a rather different understanding of the mechanism and systematics of dislocation motion than what one might have inferred from Whitehead's experiments alone.[9] Several remarks are in order. Whitehead worked in the range $1 \lesssim \epsilon \lesssim 20$ and had appreciable scatter at the lower end of this scale, whereas we concentrated on $\epsilon \lesssim 1$ in order to compare with analytic theory. Our velocities in Table III for $\epsilon = 1, 2, 4$ are, however, by no means linear though our values are comparable to Whitehead's for $\epsilon \sim 1$, $P \sim 100$. There is no hard argument why free-slip and rigid boundary conditions should give similar results except at low ϵ where an amplitude expansion is valid. For large P, however, we see no physical reason for a qualitative difference that could be attributed to the boundary conditions below ϵ of order 10, at which point other secondary instabilities occur.

It is also possible that convective effects associated with the vertical vorticity determine the defect velocity for moderate P and $\epsilon \gtrsim 1$ as Whitehead conjectured. The amplitude equation clearly cannot account for the Prandtl number dependence of the velocities for $P \lesssim 60$ and $\epsilon = 0.5$ in Table II. There is also evidence that the infinite Prandtl number limit is not approached uniformly in ϵ.

The most obvious difference between our experiments and Whitehead's is the choice of initial conditions. Some care is required for $\epsilon \sim 1$ to obtain two wavelengths in the ratio of 2 : 3 that are both stable. Our attempts in this direction for $P = \infty$ while not systematic, gave much lower velocities than we otherwise found and more in line with Whitehead's numbers at $P = 10^4$ scaled down to $\epsilon \sim 1$. We interpret our results by analogy to what we found in a larger system, $7 \leftrightarrow 6$ rolls, when the background was dilated. There, the velocity decreased and ultimately changed sign which we take as an indication that there is some wavelength that minimizes the potential F. The system will add or expel an extra roll if it can thereby lower F. When we ran $3 \leftrightarrow 2$ rolls, the two wavelengths involved, we infer, simply straddled the optimal one and resulted in a small velocity. This explanation will not suffice for Whitehead's data, since a rather large range of ϵ was explored, but clearly the initial configuration is an important determinant of the subsequent behavior and it would be interesting to see this parameter varied in future laboratory experiments.

Our defects were always observed to move parallel to the local roll axis. In the metallurgical literature this motion would be termed climb while motion perpendicular to the axis of the extra roll is called glide.[8] Glide motion could possibly be observed by preparing an initial configuration, which could only relax by dislocation glide.

Any laboratory experiment is necessarily performed in a finite container with rigid sidewalls. It has recently been shown that the presence of lateral boundaries severely restricts the possible stationary states of convection in two dimensions.[14] The dynamical means of adjusting the roll wavelength implicit in Ref. 14 is lateral diffusion followed by annihilation or creation of a roll at the wall. To lowest order in ϵ, the theory of Ref. 14 predicts a unique state at $q = q_0 + O(\sqrt{\epsilon})$ while our calculation, to the same order in ϵ, suggests that a defect will move in such a direction so as to push the roll pattern toward $q = q_0$. Our analytic calculation in Sec. III should also apply to an extra roll segment normal to a wall provided it exceeds $\xi_\perp$ in length.

To next order in $\epsilon^{1/2}$ for large P, Ref. 14 predicts there will be a band of stationary states with $q - q_0 \sim O(\epsilon)$ that bracket q_0. To this order in ϵ, the dynamics are no longer purely relaxational and we have no analytical evidence for how the sign of the dislocation's velocity depends on $q - q_0$. *A priori*, we see no reason why the defect must push the system toward the stationary states found in two dimensions.[14] To the extent it does not, and if a way can be found to nucleate new defects, one might conceivably have a source of low-frequency noise.[16]

It does seem clear that starting from imposed initial conditions, the presence of walls is only manifest on the scale of a lateral diffusion time. Since defects move ballistically, there should be a window of times in a large container during which defects can be studied free of interference from the walls. To compare with theory, it seems essential to control the initial conditions by imposing an ordered roll pattern with a fixed wavelength as discussed by Chen and Whitehead.[17] It would also be quite sensible to study defects in the presence of walls numerically by solving the amplitude equations with appropriate boundary conditions.

Several experimental groups have searched for systems analogous to Rayleigh-Bénard convection that would enable them to observe pattern changes on shorter time scales than is possible with the Boussinesq equations and to work with larger aspect ratios.[18] We claim, however, that if one is willing to initialize with an imposed planform, there is a range of interesting effects to be seen on times of order several hundred vertical thermal diffusion times. In particular, the defect velocities we found in Eq. (3.11b) for rigid boundaries, $v = 1.0\delta q^{3/2}$ with $\beta = 0.84$, $P = \infty$, and in units $\kappa = d = 1$, should be readily observable for a wide range of parameters. Laboratory verification of (3.11b) would be a more sensitive test of the amplitude equations than other recent experiments have provided.[19] It also seems quite feasible to build a well regulated cell that is comparable in size to what we could comfortably simulate numerically near onset, $68 \times 34 \times 1$. The strongest argument in favor of convection is 100 years of experience with the wealth of phenomena that can arise from such a simple statically stressed nonlinear system.

Note added in proof. We have recently shown that the amplitude equation to the order considered in Ref. 4 is incomplete and misleading for free-slip boundaries and small to moderate Prandtl numbers. The theory of Sec. III is only correct for large P.

ACKNOWLEDGMENTS

We would like to thank S. A. Orszag for making available to us his Boussinesq code and F. Busse, J. Gollub, J. Herring, and J. Whitehead for a number of helpful conversations. Our numerical simulations were performed at the National Center for Atmospheric Research which is sponsored by the N.S.F. E.D.S. was supported by a Sloan Foundation fellowship, and together with A.Z. by the National Science Foundation under Grants Nos. ATM-8005796 and DMR-77-18329.

[1] F. H. Busse, Rep. Prog. Phys. 41, 1929 (1978).
[2] D. D. Joseph, *Stability of Fluid Motions* (Springer, Berlin, 1976).
[3] A. Schlüter, D. Lortz, and F. H. Busse, J. Fluid Mech. 23, 129 (1965).
[4] L. A. Segal, J. Fluid Mech. 38, 203 (1969); A. C. Newell and J. A. Whitehead, *ibid.* 38, 279 (1969).
[5] J. Wesfreid *et al.*, J. Phys. (Paris) 39, 725 (1978); M. C. Cross, Phys. Fluids 23, 1727 (1980).
[6] F. H. Busse and J. A. Whitehead, J. Fluid Mech. 47, 305 (1971); G. E. Willis, J. W. Deardorff, and R. C. J. Somerville, *ibid.* 54, 351 (1972).
[7] E. L. Koschmieder, Adv. Chem. Phys. 26, 177 (1974).
[8] F. R. N. Nabarro, *Theory of Dislocations* (Clarendon, Oxford, 1967); P.-G. de Gennes, *The Physics of Liquid Crystals* (Oxford University Press, London, 1974); J. Friedel, *Dislocations* (Addison-Wesley, Reading, Mass., 1964); J. Toner and D. R. Nelson, Phys. Rev. B 23, 316 (1981).
[9] J. A. Whitehead, J. Fluid Mech. 75, 715 (1976).
[10] G. Ahlers and R. W. Walden, Phys. Rev. Lett. 44, 445 (1980); R. P. Behringer *et al.* (unpublished).
[11] It is difficult to determine who is responsible for these ideas; see Refs. 1 and 7.
[12] F. H. Busse, J. Fluid Mech. 52, 97 (1972).
[13] F. H. Busse and R. M. Clever, J. Fluid Mech. 91, 319 (1979); R. M. Clever and F. H. Busse, *ibid.* 65, 625 (1974).
[14] M. C. Cross *et al.*, Phys. Rev. Lett. 45, 898 (1980); and unpublished.
[15] G. K. Batchelor, *An Introduction to Fluid Mechanics* (Cambridge University Press, London, 1974), p. 535; G. S. Deem and N. J. Zabusky, Phys. Rev. Lett. 40, 859 (1978).
[16] The authors are indebted to M. C. Cross for this remark.
[17] M. M. Chen and J. A. Whitehead, J. Fluid Mech. 31, 1 (1968).
[18] E. Guazzelli (unpublished); J. P. Gollub, in *Systems Far From Equilibrium*, edited by L. Garrido (Springer, Berlin, 1980), p. 162.
[19] J. E. Wesfreid and V. Croquette, Phys. Rev. Lett. 45, 634 (1980).